APL Materials

Strain tuning of Néel temperature in $YCrO_3$ epitaxial thin films

Cite as: APL Mater. **10**, 081101 (2022); https://doi.org/10.1063/5.0095742
Submitted: 12 April 2022 • Accepted: 27 June 2022 • Published Online: 02 August 2022

Jin Hong Lee, Lourdes Marcano, Raphaël Aeschlimann, et al.

Strain tuning of Néel temperature in $YCrO_3$ epitaxial thin films

Cite as: APL Mater. 10, 081101 (2022); doi: 10.1063/5.0095742
Submitted: 12 April 2022 • Accepted: 27 June 2022 •
Published Online: 2 August 2022

View Online Export Citation CrossMark

Jin Hong Lee,[1,2] Lourdes Marcano,[3,4] Raphaël Aeschlimann,[2] Mohamad-Assaad Mawass,[3] Chen Luo,[3,5] Alexandre Gloter,[6] Julien Varignon,[7] Florin Radu,[3] Sergio Valencia,[3] and Manuel Bibes[2,a)]

AFFILIATIONS

[1] Center for Spintronics, Korea Institute of Science and Technology (KIST), 02792 Seoul, Korea
[2] Unité Mixte de Physique, CNRS, Thales, Université Paris-Saclay, 91767 Palaiseau, France
[3] Helmholtz-Zentrum Berlin für Materialien und Energie, Albert-Einstein-Straße 15, 12489 Berlin, Germany
[4] Dpto. Electricidad y Electrónica, Universidad del País Vasco-UPV/EHU, 48940 Leioa, Spain
[5] Physik-Department, Technische Universität München, 85748 Garching b. München, Germany
[6] Laboratoire de Physique des Solides, CNRS, Université Paris-Saclay, 91405 Orsay, France
[7] Laboratoire CRISMAT, CNRS UMR 6508, ENSICAEN, Normandie Université, 14050 Caen, France

[a)] **Author to whom correspondence should be addressed:** manuel.bibes@cnrs-thales.fr

ABSTRACT

Epitaxial strain is a useful handle to engineer the physical properties of perovskite oxide materials. Here, we apply it to orthorhombic chromites that are a family of antiferromagnets showing fruitful functionalities as well as strong spin–lattice coupling via antisymmetric exchange interaction along Cr–O–Cr bonds. Using pulsed laser deposition, we grow $YCrO_3$ thin films on various substrates imposing strain levels in the range from −1.8% to +0.3%. The films are stoichiometric with a 3+ valence for Cr both within the films and at their surface. They display an antiferromagnetic spin order below their Néel temperature, which we show can be strongly tuned by epitaxial strain with a slope of −8.54 K/%. A dimensionless figure of merit (defined as the slope normalized by the Néel temperature of bulk) is determined to be 6.1, which is larger than that of other perovskites, such as manganites (5.5), ferrites (2.3), or nickelates (4.6). Density functional theory simulations bring insight into the role of Cr–O bond lengths and oxygen octahedral rotations on the observed behavior. Our results shed light on orthorhombic chromites that may offer an energy-efficient piezo-spintronic operation.

Since the absence of net magnetization in antiferromagnets (AFMs) hinders their control by an external magnetic field, the spin–lattice coupling emerges as an essential mechanism to tune their properties and extends their applicability range in spintronic and magnonic devices.[1] Among a variety of approaches to harness antiparallel spin configurations in AFMs,[2] a strain-mediated control has the advantage of low-power and magnetic-field-free spintronic operation, for example, when combined with piezoelectric materials[3] or in ultrafast experiments.[4] Understanding the effect of strain in different types of AFM materials is, thus, important, particularly in noncollinear AFMs, in which recent studies revealed exotic spintronic phenomena.[3,5]

Noncollinear magnetic orthorhombic chromites[6] not only display a wide spectrum of spin configurations[7] but also possible multiferroic properties.[8] $YCrO_3$ (YCO) is a relatively simple member of the orthorhombic chromite family in which only Cr ions carry a magnetic moment. It is a canted AFM displaying weak ferromagnetism and a Néel temperature T_N ~ 141 K.[6,8] Recently, Pal *et al.*[9] showed that epitaxial YCO thin films can be grown on $(LaAlO_3)_{0.3}(Sr_2TaAlO_6)_{0.7}$ (LSAT) substrates but pointed to the difficulty of suppressing Cr species with oxidation states higher than the nominal 3+. Paudel *et al.* explored the role of substrate-induced strain on the magnetization of YCO films but their films were partially relaxed, complicating the analysis of the results.[10] So far, the

influence of epitaxial strain on the Néel temperature of YCO films has not been investigated.

In this article, we study the structural and magnetic properties of YCO epitaxial thin films grown on various substrates by performing x-ray diffraction (XRD), high-angle annular dark-field (HAADF) and annular bright field (ABF) scanning transmission electron microscopy (STEM), first-principles density functional theory (DFT) calculations, x-ray absorption spectroscopy (XAS), and superconducting quantum interference device (SQUID) magnetometry. The orthorhombic domain structure and Cr valence state of YCO thin films on $LaAlO_3$ substrates (LAO that induces the smallest misfit strain to YCO) are analyzed confirming the high growth quality. Then, we study the strain effect on the AFM transition temperature of YCO by comparing YCO thin films grown on $YAlO_3$ (YAO), $NdAlO_3$ (NAO), LAO, and $SrLaGaO_4$ (SLGO) substrates. The relation between the strain-induced changes in oxygen octahedral rotations, bond lengths, and the Néel temperature is understood by performing DFT calculations.

Epitaxial YCO thin films were epitaxially grown on four different perovskite substrates by using pulsed laser deposition (PLD). The film thickness ranged between 10 and 20 nm. The base pressure of the PLD chamber was below 10^{-7} mbar. During the YCO growth, the substrate temperature and O_2 pressure were kept at 700 °C and 0.4 mbar, respectively. The surface of a YCO pellet was ablated by 248 nm KrF excimer laser pulses. The laser fluence and repetition rate were ~2 J cm^{-2} and 5 Hz, respectively. The growth mode and quality of YCO were monitored by utilizing the reflection high-energy electron diffraction (RHEED); the YCO growth mode was initially layer-by-layer and slowly became step-flow. After the growth, the YCO films were cooled down to room temperature under the same O_2 pressure. Then, the samples were transferred in ultra-high vacuum to a *dc* magnetron sputter chamber in order to cap them with a Pt layer to prevent oxidation or degradation of the samples. The thickness of Pt was chosen between 1 and 3 nm depending on the type of measurement. The STEM measurements were performed on a Nion Cs-corrected microscope operated at 100 keV. HAADF- and ABF-STEM images were obtained for a converge semi-angle of 30 mrad with collection semi-angles between 80–200 mrad and 15–30 mrad, respectively. Electron energy loss spectroscopy (EELS) was obtained with the same microscope using a MerlinEM detector from Quantum Detectors. The XAS signals were obtained in the total electron yield (TEY) mode under the normal incidence of linearly polarized light at the VEKMAG end station installed at the PM2 beamline in BESSY II of the Helmholtz-Zentrum Berlin.[11] The high-resolution XRD data and reciprocal space maps (RSMs) were acquired by employing an x-ray four-circle diffractometer (Panalytical Empyrean) with Cu $K\alpha_1$ radiation. By using SQUID magnetometry, the Néel temperature of the samples was determined during a warm-up process in 10–50 Oe. The DFT calculations were performed with the VASP package[12,13] using the parameter free SCAN exchange-correlation functional[14] that is fully able to capture the physics of transition metal oxide perovskites.[15] The energy cut off was set to 500 eV. In order to identify the ground state with epitaxial strain, we checked two different growth orientations of $YCrO_3$ with either the $a^0a^0c^+$ rotation along or orthogonal to the substrate, thereby producing $a^+a^-c^-$ or $a^-a^-c^+$ tilt patterns for the two possible growth orientations, respectively. Then, two lattice parameters were imposed to those of the substrate, and the third parameter was allowed to relax both in magnitude and angle. In any case, atomic positions were relaxed until forces acting on each atom are lower than 1 meV/Å. Magnetic exchange interactions J were extracted by mapping the total energy for different spin configurations at fixed ground state structure on a Heisenberg model $H = -\sum_{i<j} J_{ij} S_i S_j$ where S_i is a spin located at site i. Interactions were limited to nearest-neighbor Cr^{3+} spins with two interactions between nearest neighbors in the (ab)-plane (J_1) and along c (J_2). The T_N was computed using a mean field model with $T_N = -(S+1)S(2J_1 + J_2)/(3k_B)$ where $S = 3/2$ for a Cr^{3+} cation.

Figure 1(a) shows the orthorhombic *Pbnm* crystal structure of bulk YCO where an antiferrodistortive configuration ($a^-a^-c^+$) of CrO_6 octahedra is clearly displayed.[17] The lattice parameters of bulk YCO are known as a_o = 5.522 60 Å, b_o = 5.243 76 Å, and c_o = 7.535 55 Å, where "o" indicates orthorhombic notation.[18,19] Converting the orthorhombic lattice parameters into pseudocubic (pc) lattice parameters leads to $a_{pc} \sim 3.793$ Å and $V_{pc} \sim 54.56$ Å^3. The pseudocubic in plane lattice parameters for $(001)_{pc}$-oriented YAO, NAO, LAO, and SLGO substrates are 3.708, 3.744, 3.789, and 3.852 Å, respectively. We, thus, expect that YCO films on YAO, NAO, and LAO substrates undergo compressive misfit strain but YCO films on SLGO substrates are tensile strained. Figure 1(b) shows the atomically flat surface of a YCO thin film deposited on an LAO substrate (YCO/LAO) where the lattice mismatch is the smallest among the four substrates. The RHEED patterns of the LAO substrate and the YCO film obtained during the PLD growth [Figs. 1(c) and 1(d)] exhibit vertically aligned streaks, which confirm the high-quality two-dimensional surface. The periodicity of RHEED streaks for YCO is approximately half that for the LAO substrate [Fig. 1(d)] since the orthorhombic phase of YCO has a larger unit cell compared to the pseudocubic LAO substrate.

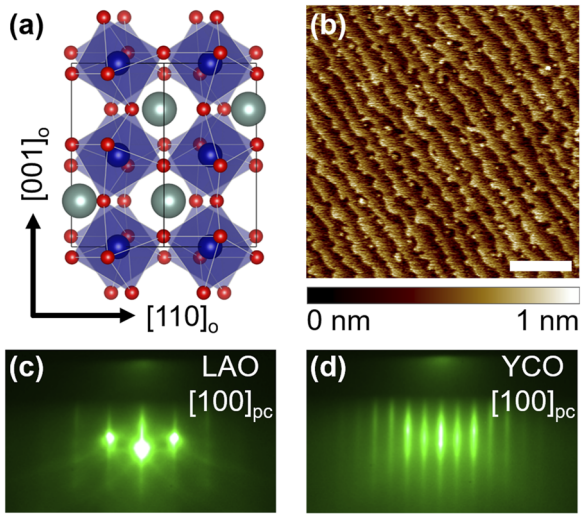

FIG. 1. (a) Orthorhombic unit-cell structure of bulk YCO.[16] (b) Atomic force microscopy image of an as-grown YCO thin film on an LAO substrate (YCO/LAO). The scale bar indicates 1 μm. RHEED pattern for the surface of (c) the LAO substrate and (d) the YCO film along $[100]_{pc}$. Here, "pc" represents the perovskite pseudocubic index and $[001]_{pc}$ defined as an out-of-plane direction.

The atomic structure of the YCO/LAO sample was investigated by performing HAADF- and ABF-STEM as summarized in Fig. 2. Figure 2(a) reveals a clear interface between the film and the substrate as well as domain boundaries along the out-of-plane orientation due to the presence of multiple structural domains in YCO. These orthorhombic YCO domains are highlighted in Fig. 2(b) and the alternating red and green domains show that the orthorhombic YCO tries to match its anisotropic in-plane lattice parameters on the pseudocubic lattice of LAO. The corresponding fast Fourier transform (FFT) images are shown in Figs. 2(c) and 2(d). Figures 2(e) and 2(f) are high-magnification ABF-STEM and HAADF-STEM images obtained in the same area, which show the sharp interface and epitaxial connection not only between YCO and LAO but also between different YCO domains.

To gain insight into the chemistry of the YCO film, EELS and XAS signals around the Cr $L_{3,2}$ edge were collected from a Pt-capped YCO/LAO sample [see Fig. 3(a)]. As the TEY mode in XAS mostly probes the surface of YCO, it is useful to compare the surface-sensitive XAS data with the EELS data obtained from the middle of the YCO layer in order to test the homogeneity of the sample along the depth direction. The shape and position of main- and sub-peaks in both spectra prove that the valence state of chromium in the YCO layer is uniformly Cr^{3+}.[20]

Using the optimized growth conditions described above, YCO thin films were epitaxially grown on three additional substrates in order to tune the strain state of YCO. The XAS spectra displayed in Fig. 3(b) indicate that all the samples have well-defined Cr^{3+} states. The lattice parameters of YCO/YAO, YCO/NAO, YCO/LAO, and YCO/SLGO samples were studied by combining conventional XRD scans [Fig. 4(a)] and high-resolution RSMs [Figs. 4(b)–4(e)]. As shown in Fig. 4(a), the $(002)_{pc}$ peak position of YCO shifts toward higher 2θ angles, i.e., toward smaller c_{pc}, as the in-plane lattice parameters of substrates increase from YAO to SLGO. By comparing the reciprocal lattice Q_x and Q_y positions between the film and substrate in the YCO/YAO sample [see dashed lines in Fig. 4(b)], one observes that YCO is fully strained along one in-plane orientation of YAO (i.e., $[001]_o$) but partially relaxed along the other orthogonal in-plane orientation (i.e., $[1\bar{1}0]_o$). Recalling that YAO also has an orthorhombic crystal symmetry, the RSM shows that the orthorhombic c_o axis of YCO is parallel and fully strained to that of YAO but the other axes are partially relaxed. Two substrate peaks appear in Fig. 4(c) due to the pronounced twin angle of NAO and a powder-like line pattern crossing near Q_z = 4.8 $Å^{-1}$ also comes from NAO but its exact origin is elusive.[21] The YCO grown on SLGO shows a broad peak feature [Fig. 4(e)], which confirms the isotropic strain of YCO on the square lattice of SLGO. Figure 4(f) summarizes the lattice parameters and unit-cell volume of YCO on the four different substrates. We see a linear scaling of the unit-cell volume (blue) as the strain state of YCO goes from compressive to tensile cases. Although the YCO film on SLGO shows some degree of structural relaxation, the T_N of this film globally falls on the same linear trend as the other samples. This suggests that, in the

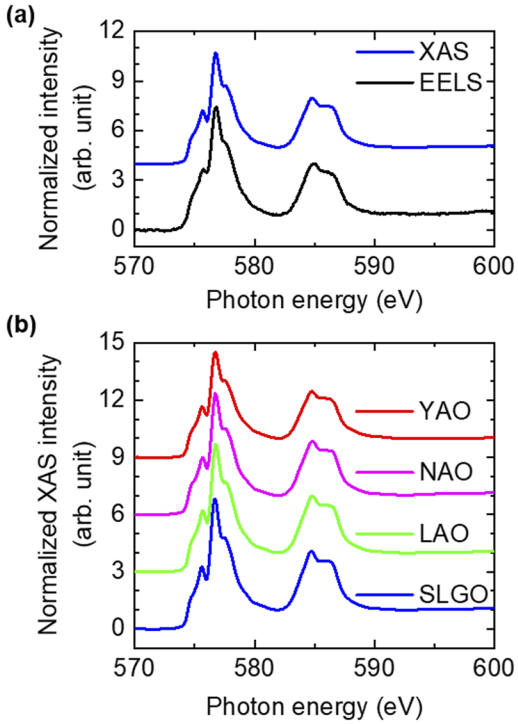

FIG. 3. (a) XAS and EELS around Cr $L_{3,2}$-edge obtained from a YCO thin film grown on an LAO substrate at room temperature. (b) XAS results from the four different samples.

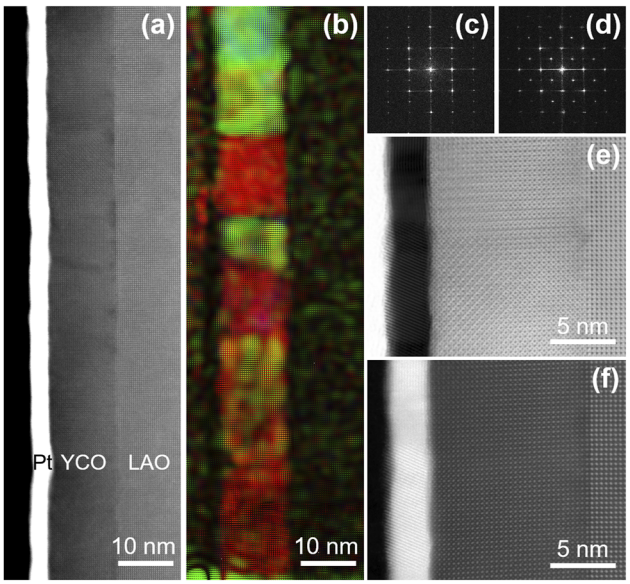

FIG. 2. (a) Low-magnification HAADF-STEM image of a YCO/LAO sample. The brightest layer on top of YCO is a Pt cap to avoid any damage during the sample preparation. (b) Composite image showing the three different crystallographic orientations (red, green, and blue domains) in the YCO layer. The green, red, and blue domains correspond to the cases where the orthorhombic b_o axis (i.e., the longest) is oriented along $[100]_{pc}$, $[010]_{pc}$, and $[001]_{pc}$. FFT image of (c) green and (d) red domains shown in (b). High-magnification (e) ABF-STEM and (f) HAADF-STEM images.

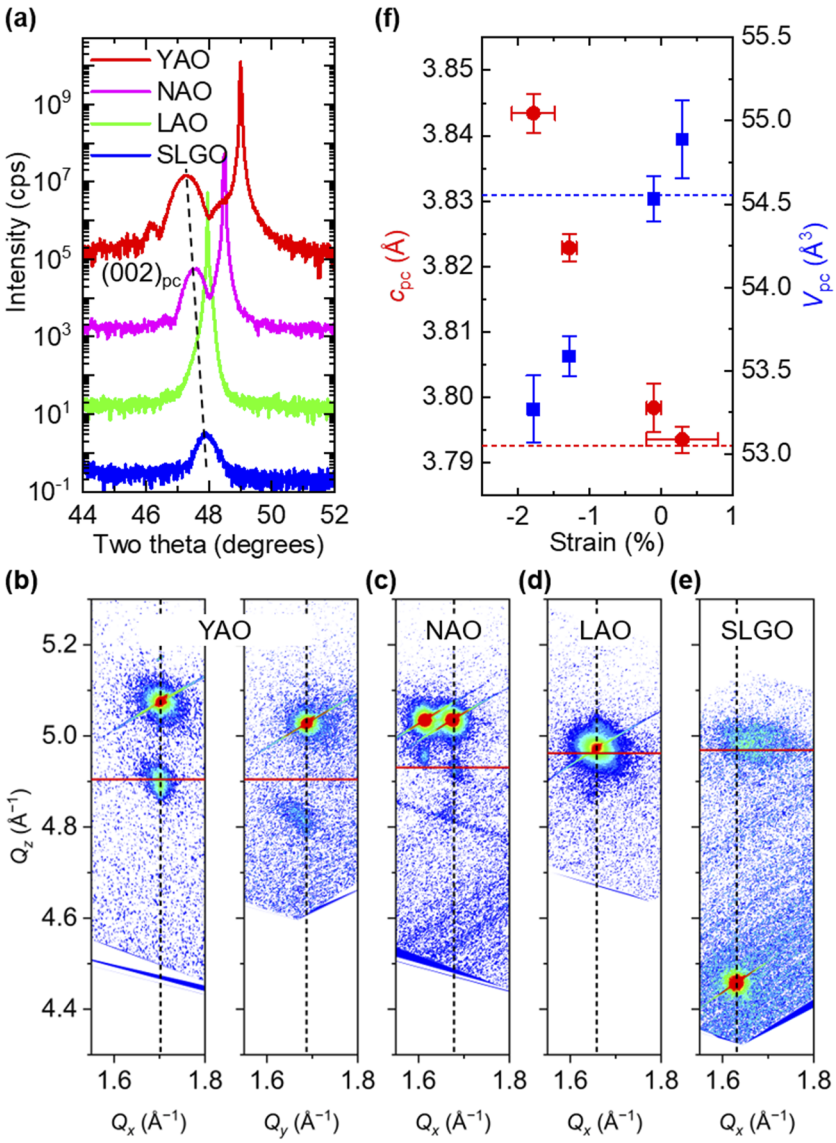

FIG. 4. (a) Conventional XRD scans showing the $(002)_{pc}$ peaks of YCO grown on four different substrates. The dashed line is a guide to the eye and indicates the systematic shifts of the YCO $(002)_{pc}$ peak. (b)–(e) RSMs around (103)pc peaks. For the YAO case, two different in-plane orientations were measured as the substrate has anisotropic in-plane lattice parameters. Here, the dashed lines represent the Q_x and Q_y positions of the intense substrate peaks. The red lines indicate the pseudocubic Q_z positions calculated from (a). (f) The strain dependence of out-of-plane lattice parameter (c_{pc}) and unit-cell volume (V_{pc}) where the dashed lines correspond to the bulk (or strain-free)[18,19] unit cell.

first approximation, defects associated with strain relaxation do not have a strong influence on the Néel temperature. However, studying the effect of dislocations or strain gradients on the functional properties of chromium perovskites is certainly worth investigating in the future.

In order to determine the Néel temperature of the samples, the canted magnetic moment (m) was measured as a function of temperature [Fig. 5(a)]. As the weak moment occurs as a result of the noncollinear AFM configuration in YCO, the onset of the non-zero magnetic moment informs on the Néel temperature.[6] The strong increase of m below ~40 K signals the paramagnetic contribution of the Pt cap. Figure 5(b) summarizes the strain-dependence of T_N in YCO thin films. The transition temperature is inversely proportional to the strain value and it is quantified by the slope of the graph to −8.54 K/%. A figure of merit (f) can be defined if we normalize the slope by T_N of bulk YCO, resulting in a useful dimensionless quantity for comparing the strain sensitivity of T_N in different materials. We obtained f = 6.1 for YCO, and interestingly, it is larger than the values estimated from the previous reports on other perovskite AFMs: f = 5.5 for $La_{0.7}Sr_{0.3}MnO_3$ (LSMO),[23] 2.3 for $BiFeO_3$,[24] and 4.6 for $NdNiO_3$[25] as shown in Fig. 5(c).

In order to get insights into the evolution of T_N with strain, the computed Néel temperature on the basis of DFT calculations is also reported in Fig. 5(b). First, we find that the bulk YCO adopts an orthorhombic structure with antiferromagnetic interaction between all nearest-neighbor Cr^{3+} spins, yielding a computed T_N of 136 K, in sharp agreement with the experimental value of 141 K.[22] Second, we identify that all tested epitaxial strain values ranging

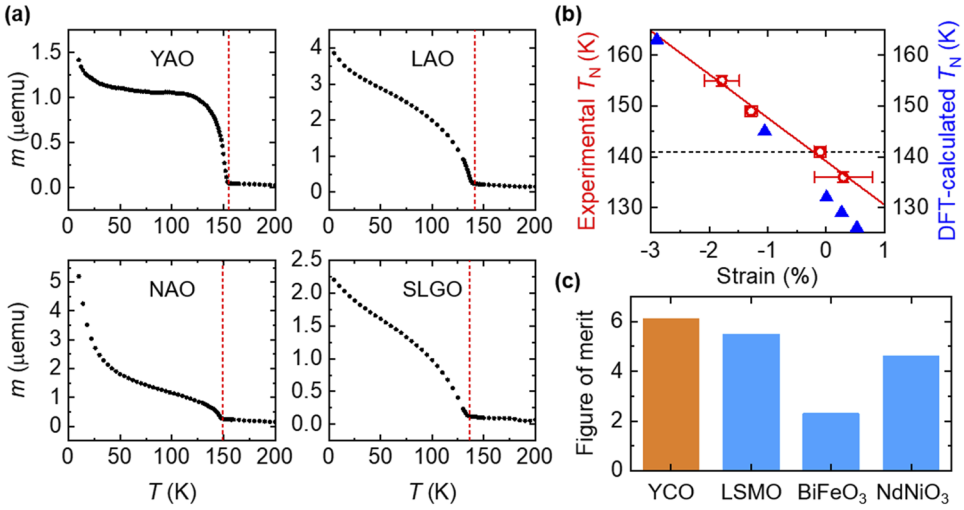

FIG. 5. (a) Temperature-dependent magnetic moment of YCO thin films on the four different substrates. The dashed lines indicate the determined Néel temperature. (b) Experimental and DFT-calculated T_N as a function of strain. The dashed line points out the reference value for a YCO single crystal.[22] (c) Figure of merit for YCO and various perovskite AFMs estimated from Refs. 23–25.

from −2.90 to +0.53% lead to a growth orientation with the $a^0a^0c^+$ rotation aligned along the substrate, hence yielding $a^+a^-c^-$ tilt patterns. The computed T_N as a function of strain follows the experimental trend, i.e., an increase of T_N with the compressive strain [see Fig. 5(b)]. This is ascribed to a monotonous (i) shortening of Cr–O bond lengths on average and (ii) weakening of the $a^+a^0c^0$ octahedral rotations when going from +0.53% to −2.90% of epitaxial strain while the $a^0a^-c^-$ rotation amplitudes are roughly constant with strain. Ultimately, superexchange is favored yielding an increase of J_1 and J_2 magnetic constants and T_N. The slight deviation of T_N between DFT and experimental results for the tensile strain may originate from minor O vacancies (i.e., not considered in the DFT calculation) generally observed in other magnetic oxide films[26,27] and whose formation is favored by the tensile strain.[28]

In conclusion, we have investigated the influence of epitaxial strain on the Néel temperature of YCO by growing YCO thin films on four different substrates ranging from compressive to tensile strain regions. The crystal structure and chemistry of YCO have been investigated in order to confirm the high quality of the samples. Without much difference in the valence state of Cr for all the samples, we have observed that the Néel temperature of YCO decreases when the in-plane lattice parameters of substrates increase. The strain engineering of Cr–O–Cr superexchange interaction has been understood with the help of DFT calculation. Our findings exemplify the strain-control of noncollinear AFM materials and infer that the compressive strain can be more reliable for improving the mechanical switching process of noncollinear AFM oxides without generating oxygen defects.

This work received support from the ERC CoG "MINT" (Grant No. 615759), the ERC AdG "FRESCO" (Grant No. 833973), the European Union's Horizon 2020 research and innovation programme under grant agreement No 964931 (projet "TSAR") and the M-Era.Net project "SWIPE". We thank the Helmholtz-Zentrum Berlin für Materialien und Energie for the allocation of synchrotron radiation beamtime. L.M. acknowledges the financial support provided through a postdoctoral fellowship from the Basque Government (Grant No. POS- 2019-2-0017). J.V. acknowledges access granted to HPC resources of Criann through Project Nos. 2020005 and 2007013 and of Cines through DARI Project No. A0080911453.

AUTHOR DECLARATIONS

Conflict of Interest

The authors have no conflicts to disclose.

Author Contributions

Jin Hong Lee: Writing – original draft (lead); Writing – review & editing (lead). **Lourdes Marcano:** Methodology (equal). **Raphaël Aeschlimann:** Methodology (equal). **Mohamad-Assaad Mawass:** Methodology (equal). **Chen Luo:** Methodology (lead). **Alexandre Gloter:** Methodology (lead). **Julien Varignon:** Methodology (lead); Writing – original draft (supporting); Writing – review & editing (supporting). **Florin Radu:** Methodology (lead). **Sergio Valencia:** Methodology (lead). **Manuel Bibes:** Writing – original draft (lead); Writing – review & editing (lead).

DATA AVAILABILITY

The data that support the findings of this study are available from the corresponding author upon reasonable request.

REFERENCES

[1] E. A. Mashkovich, K. A. Grishunin, R. M. Dubrovin, A. K. Zvezdin, R. V. Pisarev, and A. V. Kimel, Science **374**, 1608 (2021).
[2] V. Baltz, A. Manchon, M. Tsoi, T. Moriyama, T. Ono, and Y. Tserkovnyak, Rev. Mod. Phys. **90**, 015005 (2018).
[3] Z. Liu, Z. Feng, H. Yan, X. Wang, X. Zhou, P. Qin, H. Guo, R. Yu, and C. Jiang, Adv. Electron. Mater. **5**, 1900176 (2019).
[4] D. Afanasiev, J. R. Hortensius, B. A. Ivanov, A. Sasani, E. Bousquet, Y. M. Blanter, R. V. Mikhaylovskiy, A. V. Kimel, and A. D. Caviglia, Nat. Mater. **20**, 607 (2021).

[5]H. Chen, Z. Feng, H. Yan, P. Qin, X. Zhou, H. Guo, X. Wang, H. Wu, X. Zhang, Z. Meng, and Z. Liu, Phys. Rev. B **104**, 064428 (2021).
[6]E. Bousquet and A. Cano, J. Phys.: Condens. Matter **28**, 123001 (2016).
[7]I. S. Jacobs, H. F. Burne, and L. M. Levinson, J. Appl. Phys. **42**, 1631 (1971).
[8]C. R. Serrao, A. K. Kundu, S. B. Krupanidhi, U. V. Waghmare, and C. N. R. Rao, Phys. Rev. B **72**, 220101(R) (2005).
[9]B. Pal, X. Liu, F. Wen, M. Kareev, A. T. N'Diaye, P. Shafer, E. Arenholz, and J. Chakhalian, Appl. Phys. Lett. **112**, 252901 (2018).
[10]B. Paudel, Y. Sharma, B. K. Derby, G. Pilania, M. M. Schneider, A. C. Jones, H. Nakotte, M. T. Pettes, and A. Chen, Mater. Res. Lett. **10**, 29 (2022).
[11]T. Noll and F. Radu, "The Mechanics of the Vekmag Experiment," in *Proceedings of MEDSI'16*, Geneva, Switzerland, 2017, http://jacow.org, pp. 370–373.
[12]G. Kresse and J. Hafner, Phys. Rev. B **47**, 558 (1993).
[13]G. Kresse and J. Furthmüller, J. Comput. Mater. Sci. **6**, 15 (1996).
[14]J. Sun, A. Ruzsinszky, and J. Perdew, Phys. Rev. Lett. **115**, 036402 (2015).
[15]J. Varignon, M. Bibes, and A. Zunger, Phys. Rev. B **100**, 035119 (2019).
[16]K. Momma and F. Izumi, J. Appl. Crystallogr. **44**, 1272 (2011).
[17]M. C. Weber, J. Kreisel, P. A. Thomas, M. Newton, K. Sardar, and R. I. Walton, Phys. Rev. B **85**, 054303 (2012).
[18]J. Prado-Gonjal, R. Schmidt, J.-J. Romero, D. Ávila, U. Amador, and E. Morán, Inorg. Chem. **52**, 313 (2013).
[19]S. Kovachev, D. Kovacheva, S. Aleksovska, E. Svab, and K. Krezhov, AIP Conf. Proc. **1203**, 199 (2010).
[20]K. H. L. Zhang, Y. Du, P. V. Sushko, M. E. Bowden, V. Shutthanandan, S. Sallis, L. F. J. Piper, and S. A. Chambers, Phys. Rev. B **91**, 155129 (2015).
[21]C.-S. Woo, J. H. Lee, K. Chu, B.-K. Jang, Y.-B. Kim, T. Y. Koo, P. Yang, Y. Qi, Z. Chen, L. Chen, H. C. Choi, J. H. Shim, and C.-H. Yang, Phys. Rev. B **86**, 054417 (2012).
[22]V. M. Jüdin and A. B. Sherman, Solid State Commun. **4**, 661 (1966).
[23]C. Adamo, X. Ke, H. Q. Wang, H. L. Xin, T. Heeg, M. E. Hawley, W. Zander, J. Schubert, P. Schiffer, D. A. Muller, L. Maritato, and D. G. Schlom, Appl. Phys. Lett. **95**, 112504 (2009).
[24]I. C. Infante, S. Lisenkov, B. Dupé, M. Bibes, S. Fusil, E. Jacquet, G. Geneste, S. Petit, A. Courtial, J. Juraszek, L. Bellaiche, A. Barthélémy, and B. Dkhil, Phys. Rev. Lett. **105**, 079901 (2010).
[25]J. Liu, M. Kargarian, M. Kareev, B. Gray, P. J. Ryan, A. Cruz, N. Tahir, Y.-D. Chuang, J. Guo, J. M. Rondinelli, J. W. Freeland, G. A. Fiete, and J. Chakhalian, Nat. Commun. **4**, 2714 (2013).
[26]D. Kumar, A. David, A. Fouchet, A. Pautrat, J. Varignon, C. U. Jung, U. Lüders, B. Domengès, O. Copie, P. Ghosez, and W. Prellier, Phys. Rev. B **99**, 224405 (2019).
[27]T. H. Kim, T. R. Paudel, R. J. Green, K. Song, H.-S. Lee, S.-Y. Choi, J. Irwin, B. Noesges, L. J. Brillson, M. S. Rzchowski, G. A. Sawatzky, E. Y. Tsymbal, and C. B. Eom, Phys. Rev. B **101**, 121105(R) (2020).
[28]U. Aschauer, R. Pfenninger, S. M. Selbach, T. Grande, and N. A. Spaldin, Phys. Rev. B **88**, 054111 (2013).